Development of a high-performance ammonium formate fuel cell

Zhefei Pan,[a] *Zhewei Zhang,*[a] *Wenzhi Li,*[a] *Xiaoyu Huo,*[a] *Yun Liu,*[a] *Oladapo Christopher Esan,*[a]

Qixing Wu,[b,*] *Liang An*[a,*]

[a] Department of Mechanical Engineering, The Hong Kong Polytechnic University, Hung Hom, Kowloon, Hong Kong SAR, China

[b] Shenzhen Key Laboratory of New Lithium-ion Batteries and Mesoporous Materials, College of Chemistry and Environmental Engineering, Shenzhen University, Shenzhen, 518060, China

*Corresponding authors.

Email: qxwu@szu.edu.cn (Qixing Wu)

Email: liang.an@polyu.edu.hk (Liang An)

ABSTRACT: Direct formate fuel cells are attractive due to their high theoretical voltage of 1.45 V, facile and complete formate oxidation in alkaline media, and ease of handling during storage and transportation. However, the presence of cations in the fuel solution only increases the weight load of fuel cell system without contributing to electricity generation. In this work, an ammonium formate fuel cell is developed, which can not only retain the advantages of formate, but also substitute the Na^+/K^+ with ammonium (NH_4^+) to release electrons for electricity generation. This fuel cell achieves a peak power density of 61 mW cm^{-2} at 60 ºC. By replacing pure oxygen with hydrogen peroxide and increasing the temperature and fuel concentration, the peak power density is boosted to 337 mW cm^{-2}. In addition, a mathematical model incorporating mass/charge transport and electrochemical reactions is developed to illustrate the voltage losses.

TOC GRAPHICS

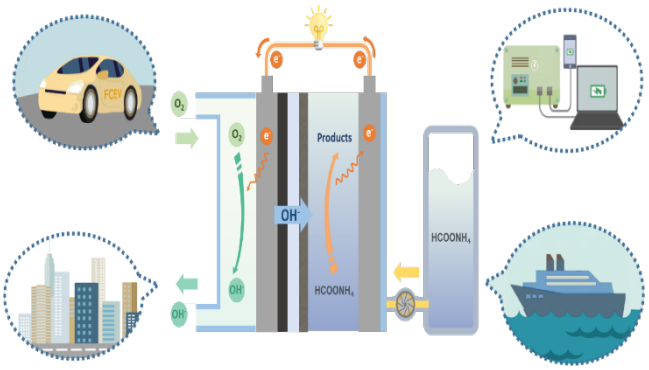

Direct liquid fuel cells fueled by molecules such as methanol, ethanol and formate, have received considerable attention as proton exchange membrane fuel cells on account of their compact fuel cartridge, uncomplicated structure, superior energy density, and ease of fuel storage and transport.[1-4] Among them, formate, particularly sodium formate or potassium formate, has gained growing attention because of its advantageous characteristics, including a high theoretical voltage of 1.45 V, facile and complete formate oxidation in alkaline media, and easy handling in storage and transportation.[5, 6] Formate is a carbon-neutral fuel that can be easily derived from the reduction of carbon dioxide via artificial photosynthesis.[7] Unlike in acid media, there is no poisoning effect for the formate oxidation in alkaline media, making the process facile in alkaline, particularly on the palladium (Pd).[8] The theoretical voltage of formate fuel cell is 0.24 V and 0.31 V higher than the fuel cells running on methanol and ethanol, respectively.[9] However, the presence of cations (Na^+ or K^+) in the fuel solution does not contribute to electricity generation and only increase the weight load of the fuel cell system, lowering the energy density of formate to 2.1 kWh L^{-1}.[10] In this work, ammonium formate is adopted as the fuel, which not only retains the advantages of formate, but also substitutes the Na^+/K^+ with ammonium (NH_4^+) which can also be oxidized to release electrons for electricity generation.[11-13] As a result, the energy density ammonium formate is upgraded to 3.2 kWh L^{-1}.[14, 15] The membrane is an indispensable component in a fuel cell. Anion exchange membranes (AEMs) contain positively charge head groups in the membrane which permit the passage of anions while repelling cations.[16] The use of an AEM creates an alkaline environment, and therefore, offers several advantages: enhanced oxygen reduction catalysis,

allowing for the use of less expensive catalysts, extended range of cell and stack materials stable in the fuel cell environment, and a wider range of less expensive polymer chemistry (fluorinated raw materials are not necessary).[17]

The development of ammonium formate fuel cells has been hampered by various technical challenges, including sluggish kinetics and electrode degradation during ammonium formate oxidation.[18, 19] To address this issue, previous studies have investigated the use of different catalysts to boost the activity of Pt electrodes. Ohyama et al.[20, 21] found that adding Ir to Pt electrodes improved the activity of ammonium formate oxidation, while Aoki et al.[22] demonstrated that adding Ru enhances ammonium oxidation through the dehydrogenation steps of ammonia at a potential. However, it is important to note that these electrochemical performances were evaluated at the electrode scale using a three-electrode system. To date, no ammonium formate fuel cell has been developed, and the electrochemical performance at the cell scale remains to be evaluated. The mechanism of formate oxidation in the alkaline electrolyte is similar to that in the acid electrolyte, which is applicable for both Pd and Pt. For Pd, it goes through the direct oxidation pathway that the adsorbed formate first decomposes into two fragments such as H_{ad} and CO_{2ad}^{-}, and CO_{2ad}^{-} is further oxidized by OH^{-} to CO_3^{2-}.[23] For Pt, the formate oxidation is slightly active, and follows a dual-pathway mechanism, which is analogous to formic acid oxidation in acid media.[24] To tackle these issues, we have synthesized a bimetallic PtPd/C electrocatalyst using a facile chemical reduction method with sodium borohydride as the agent.[25] The reason for introducing Pt to Pd and using the PtPd catalyst is that Pt is the most active one for ammonium

oxidation due to its appropriate adsorption of intermediate and steady-state activity.[26] The PtPd/C electrocatalyst exhibits superior electrocatalytic activity for ammonium formate oxidation compared to pure Pt/C and Pd/C. An ammonium formate fuel cell, consisting of a PtPd/C anode, a Pt/C cathode, and an AEM, is therefore developed and tested. The ammonium formate oxidation reaction (AFOR) can be represented by Eq. 1. This reaction takes place on the anode, where the electrons are transferred to an external circuit to generate electricity. The products of the reaction include carbonate, nitrogen, and water. The water then travels across the AEM to the cathode, where it participates in the oxygen reduction reaction (ORR), as represented by Eq. 2. The overall reaction of the fuel cell is the combination of the AFOR and ORR (Eq. 3).

$$HCOONH_4+7OH^- \rightarrow CO_3^{2-}+1/2N_2+6H_2O+5e^- \qquad E_{AFOR} = -0.91\ V \qquad (1)$$

$$O_2+2H_2O+4e^- \rightarrow 4OH^- \qquad E_{ORR} = 0.4\ V \qquad (2)$$

$$HCOONH_4+5/4O_2+2OH^- \rightarrow CO_3^{2-}+1/2N_2+7/2H_2O \qquad E^0 = 1.31\ V \qquad (3)$$

It is shown in Figure S1 that the potential side products (NO_2^- and NO_3^-) are quantified as the NO_x will dissolve in the alkaline solution.[27, 28] It is proved that the side products of NO_x exit during electro-oxidation of ammonium formate. We have tried to determine the amounts of potential products: NO_2^- and NO_3^- via ion chromatography, HCO_3^- and CO_3^{2-} via titration). Interestingly, CO_3^{2-} is not detected or its concentration is below the quantification limit. Since the amount of N_2 is too small to collect, its amount is presumably estimated from the coulomb conservation by only subtracting the total amount of NO_2^-, NO_3^- and HCO_3^- (Figure S1). Hence, the selectivity of ammonium oxidation can be obtained: 1.1% for NO_2^-, 19.8% for NO_3^-, and 79.1% for N_2, and the

selectivity of ammonium formate oxidation can be quantified: 0.3% for NO_2^-, 5.6% for NO_3^-, 11.2% for N_2, and 82.9% for HCO_3^-. Since the production rates of NO_2^- and NO_3^- is relatively small, its influence on the potential might be minor (slightly positive shift). Further precise detection should be performed to confirm the production rate of N_2 for in-depth understanding on the selectivity in the present fuel cell. The economic analysis is made according to the fuel cell assembly and fuel cell operation as summarized in Table S1. It can be seen that the majority of cost is derived from the fuel cell assembly rather than the fuel cell operation. Although the base is necessary for maintaining the high pH, the cost of KOH supply is not an issue.

The morphology of PtPd/C nanoparticles was characterized using scanning electron microscopy (SEM), X-ray diffraction (XRD), transmission electron microscopy (TEM), and X-ray photoelectron spectroscopy (XPS). According to the SEM image in Figure 1a, the carbon particles exhibit a uniform distribution of Pt and Pd elements, which facilitates to enhance exposure of active sites for electrochemical reactions. The XRD results shown in Figure 1b reveal that primary diffraction peaks detected for the (111), (200), and (220) facets of PtPd/C occur at angles of 39.56°, 46.02°, and 67.31°, respectively.[29] These peaks are located between the typical peaks of Pt and Pd, suggesting that it is a bimetallic state. TEM images further confirm the dominant (111) facet of both Pt and Pd, with interlayer spacing of 0.229 nm and 0.225 nm in Figure 1c, respectively, consistent with the XRD pattern. The XPS spectra of PtPd/C represented in Figures 1d and 1e show the binding energies of 70.88 eV and 74.08 eV, corresponding to the Pt $4f_{7/2}$ and Pt $4f_{5/2}$,

respectively, which can be divided into two peaks at around 70.67 eV and 71.34 eV, as well as 74.03 eV and 74.69 eV, indicating the presence of Pt metal and PtO species.[30] The peak intensity suggests that Pt metal is the predominant species. The peaks at around 335.16 eV and 337.00 eV, as well as 340.38 eV and 342.28 eV, correspond to the Pd $3d_{5/2}$ and Pd $3d_{3/2}$, respectively, indicating the presence of Pd metal and PdO species.[31] Taken together, these characterization results confirm that PtPd/C was successfully synthesized in this work.

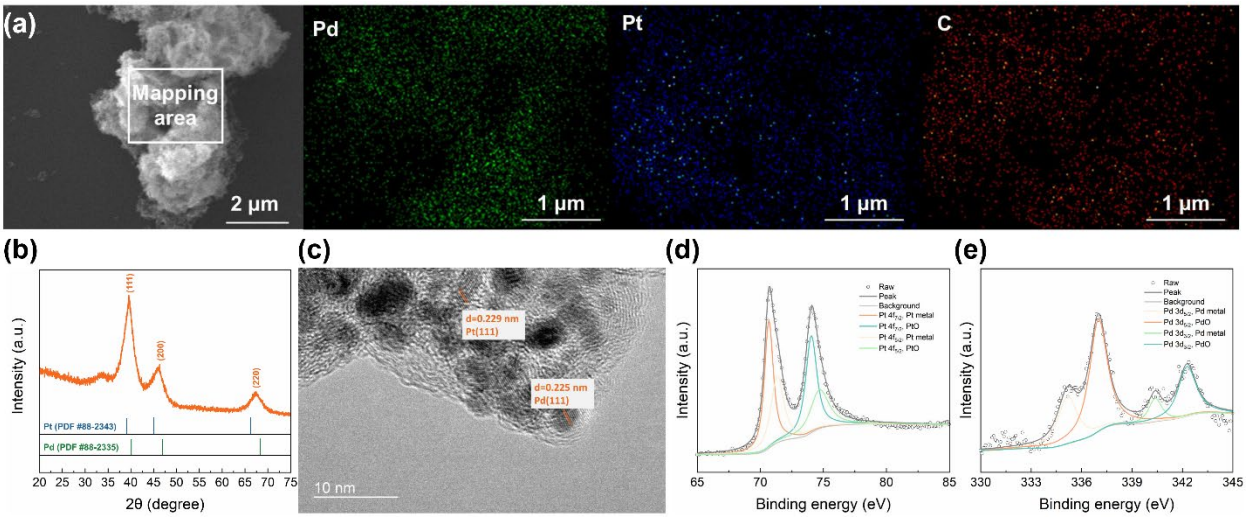

Figure 1. (a) SEM image and element mapping of prepared PtPd/C. (b) XRD pattern of prepared PtPd/C. (c) TEM image with (111) facets of Pt and Pd. (d) XPS spectra of Pt 4f. (e) XPS spectra of Pd 3d.

Figure 2a and 2b display the SEM images of PtPd/C-based three-dimensional electrodes at various scales. The images reveal that a thin film of catalyst coats the carbon cloth fiber, creating a porous structure. This structure allows for mass transport through the pores and channels, exposing the active sites on the catalyst to the reactants and initiating electrochemical reactions.

Figure 2c shows the CV of different catalyst-based electrodes in 0.1 M ammonium formate and 1.0 M KOH. The Pd-based electrode exhibited an anodic peak at around -0.2 V, which is attributed to the oxidation of formate ions. However, no peak can be observed at higher applied potentials, suggesting that the oxidation of ammonium ions does not occur due to the poor oxidation ability of pure Pd towards ammonium ions. In contrast, the pure Pt-based electrode shows two anodic peaks: the first one between -0.9 V to -0.4 V is due to the hydrogen adsorption, while the second one located at 0.1 V is mainly due to the oxidation of ammonium ions. The PtPd-based electrode displays both the formate oxidation peak and the ammonium oxidation peak, indicating its ability to achieve the complete oxidation of ammonium formate. Moreover, the current density of PtPd-based electrode is higher than that of the other electrodes, indicating catalytic activity and more intense oxidation reactions. The catalytic activity of PtPd-based electrode for different fuels (ammonium formate, formate, and ammonia) was investigated and results are depicted in Figure 2d. It is evident that the addition of fuel into 1.0 M KOH significantly boosted the current density, indicating its catalytic activity for all the fuels. At low applied potentials, the peak intensity of formate was similar to that of ammonium formate, and significantly higher than that of ammonia. At high applied potentials, the peak intensity of ammonium formate was similar to that of ammonia, and significantly higher than that of formate. Based on these results, it can be concluded that the PtPd-based electrode is most suitable for ammonium formate oxidation since its current density is promising at all applied potential regions. To verify the stability of PtPd-based electrode, the chronoamperometry (CA) is conducted (Figure S2). It can be seen that the current density is

quite stable in the 24-h test. The XRD patterns of before and after CA test also indicates that the PtPd is stable due to no obvious change is observed. In addition, the SEM and element mapping images in Figure S3 demonstrate that the morphology of electrode and the catalyst distribution are similar as well.

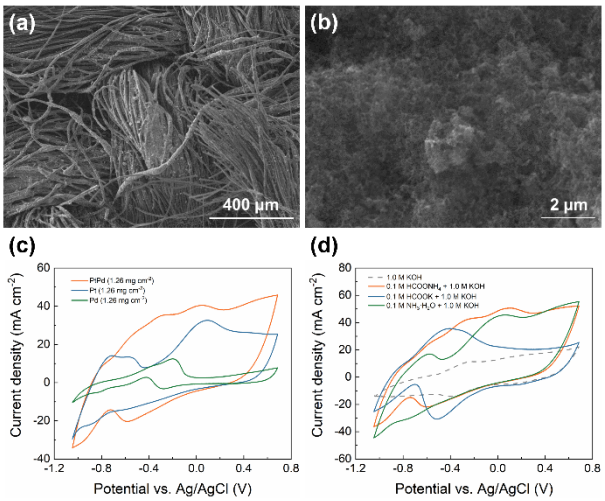

Figure 2. (a) SEM images of PtPd/C-based electrode (400 μm). (b) SEM images of PtPd/C-based electrode (2 μm). (c) CV results of different electrodes in 0.1 M ammonium formate and 1.0 M KOH solution. (d) CV results of PtPd/C-based electrode in different fuels and 1.0 M KOH solution.

The fuel cell was fed with a fuel solution of 3.0 M fuel (ammonium formate, formate and ammonia) and 3.0 M KOH flowing at 1.0 mL min^{-1} as well as pure oxygen at a flow rate of 10 SCCM at 60 °C. The polarization and power density curves are presented in Figure 3a. The ammonium formate fuel generated a peak power density of 61 mW cm^{-2} and an open-circuit voltage (OCV) of 0.88 V, while the formate fuel produced a peak power density of 74 mW cm^{-2} and an OCV of 0.85 V. In contrast, the ammonium fuel only yielded a peak power density of 5 mW cm^{-2} and an OCV of 0.77

V. The worst performance of ammonia can be attributed to two reasons: one is the intrinsic poor catalytic activity of PtPd for ammonia oxidation, and the other is the low operating temperature of fuel cell; the operating temperature should be beyond 90 ºC to obtain a faster ammonia oxidation kinetics and a better cell performance.[32, 33] The ammonium formate fuel cell exhibited an inferior peak power density compared to that of the formate fuel cell. This is because of the anode potential at the low region, such that the PtPd-based electrode catalyzes the formate oxidation more efficiently, as demonstrated by the CV results depicted in Figure 2d.[34] Although the performance of ammonium formate fuel cell is a little lower, the energy efficiency may exceed the formate fuel cell as explained previously that the cations in the fuel solution do not contribute to electricity generation. These two conjectures will be verified by detecting the operando anode potential and conducting constant-current discharging, which will be presented and discussed later. Recent studies have demonstrated that hydrogen peroxide (H_2O_2) as an alternative oxidant has remarkable advantages: it increases the fuel cell theoretical voltage thus improving performance and it enables the fuel cell to operate with the absence of oxygen environment, such as underwater and space conditions. Particularly, hydrogen peroxide offers many other advantages compared with oxygen, such as the low activation loss of the reduction reaction due to two-electron transfer and no water flooding problem. It also should mention that hydrogen peroxide is a clear liquid with an irritating odor and a low vapor pressure, and exposure to higher concentrations can come with risks if a person ingests, inhales, or gets it on their skin or in their eyes. Although hydrogen peroxide is not combustible, it may cause fire or explosion when contacting/reacting with other substances and

thus special caution must be taken to deal with it. Therefore, to further boost the fuel cell performance, the pure oxygen is replaced by hydrogen peroxide, leading to the creation of an acid-alkaline ammonium formate fuel cell with a theoretical voltage as high as 1.86 V while the alkaline ammonium formate fuel cell only has a theoretical voltage of 1.28 V. The overall reaction is shown below:[35]

$$2HCOONH_4+4OH^-+5H_2O_2 \rightarrow 2CO_3^{2-}+N_2+12H_2O \quad E=1.86\,V \tag{4}$$

The calculation of the theoretical voltage should account for the junction potential (-0.83 V v.s. SHE at 25 °C)[36] for dissociation of water in the alkaline/acid interface (anode electrode/Nafion membrane in our work) and the detailed calculation is shown in the Supporting Information. This improvement in theoretical voltage creates plenty room for performance enhancement. Figure 3b displays the fuel cell's polarization and power density curves, operating with a 3.0 M ammonium formate and 3.0 M KOH fuel solution flowing at a rate of 1.0 mL min^{-1}, and a 1.0 M H_2SO_4 and 4.0 M H_2O_2 oxidant solution flowing at a rate of 2.0 mL min^{-1} at 60°C. The results show that the fuel cell achieved a peak power density of 100 mW cm^{-2} and an OCV of 1.31 V, which is significantly higher than the results achieved with pure oxygen (61 mW cm^{-2} and 0.88 V at 60 °C). By increasing the operating temperature from 60 °C to 90 °C, the fuel cell's power density impressively increased to 188 mW cm^{-2}, despite a decrease in OCV from 1.31 V to 1.24 V. When maintaining the operating temperature at 90 °C, the peak power density can be continuously promoted by feeding higher-concentration ammonuam formate (Figure 3b). The OCV becomes

lower with higher feeding concentrations, which is reasonable and attributed to the ammonium formate crossover to the cathode, causing the mixed potential and diminishing the cell voltage.[37] The positive effect in enhancement of power density overweighs the negative effect in reducing OCV, and thus the peak power density reaches 337 mW cm^{-2} with 5.0 M ammonium formate. However, further increasing the ammonium foramte concentration does not present a continuous enhancement. This is because of the competitive adsorption of reactants, leading the other reactants at starvation states. Although the maximum power densities were comparable between the ammonium formate fuel cell with pure oxygen and the formate fuel cell, our focus now shifts to examining the efficiency. To confirm our hypothesis, we conducted a constant-current discharging test to determine the Faradaic efficiency, energy efficiency, and gravimetric energy density in this system. Figure 3d presents the discharging behavior at a current density of 75.0 mA cm^{-2} and a temperature of 60 ºC. It can be observed that the formate fuel cell exhibits the shortest discharging time of 1.3 h. Based on the discharging current and duration, the Faradaic efficiency can be calculated by Eq. 5.[38]

$$\text{Faradaic efficiency} = \frac{\text{Discharging capacity} \times 3600}{n \times V \times N \times F} \quad (5)$$

where *n* is the fuel concentration, *V* is the volume of fuel solution, *N* is the number of electrons released by one molecule of fuel, and *F* is the Faraday constant. Hence, the Faradaic efficiency of formate fuel cell is 6.2%. Although the ammonium formate fuel cell experiences a severe voltage degradation at the initial state compared to formate fuel cell, the discharging time is dramatically increased to 37.4 h. Hence, the Faradaic efficiency of formate fuel cell is boosted to 69.9%, which

is significantly higher than the Faradaic efficiency of formate fuel cell. When hydrogen peroxide is used as oxidant, the Faradaic efficiency is 61.8%, which is almost the same as the condition where pure oxygen is used as oxidant, despite a slight decrease due to the discharging time. Integrating the transient voltage can thus contribute to calculating the energy efficiency by Eq. 6.[38]

$$\text{Energy efficiency} = \frac{\text{Discharging capacity} \times 3600}{n \times V \times N \times F} \times \frac{\sum V(t)dt}{E^0 \times t} \quad (6)$$

where $V(t)$ is the transient voltage, and E^0 is the theoretical voltage. Therefore, the energy efficiency of formate fuel cell is 2.6%. Since the ammonium formate fuel cell discharges longer, its energy efficiency reaches 6.4%, which is three times higher than formate fuel cell. The energy efficiency of ammonium formate-hydrogen peroxide fuel cell reaches 23.2%. The impressive improvement is attributed to the sustained high voltage during the discharging process. The energy efficiencies of state-of-the-art direct liquid fuel cells (formic acid, methanol, ethanol, ethylene glycol, and sodium borohydride) are summarized in Table S2. The gravimetric energy density of fuels in this system can be calculated by Eq. 7.

$$\text{Gravimetric energy density} = \frac{\text{Discharging energy} \times 3600}{n \times V \times M} \quad (7)$$

where M is the molecular weight of fuels. The energy densities of formate and ammonium formate fuel cell are 69 J g^{-1} and 629 J g^{-1}, respectively. It is boosted to 1892 J g^{-1} when using hydrogen peroxide. The gravimetric energy density of ammonium formate fuel cell is sixteen times higher than that of formate fuel cell, which can further elucidate the significant difference in efficiency between the ammonium formate fuel cell and formate cell. Note that if the total mass of fuel and oxidant is sufficiently larger than the fuel cell, the mass of the fuel cell fixture or stack becomes

minor, especially for large-scale applications. Hence, the theoretical gravimetric energy density of ammonium formate fuel cell with hydrogen peroxide should be lower than that with ambient oxygen (without accounting for its mass), though the theoretical voltage of the former is ~1.4 times of the latter. However, this work mainly focuses on the Faradaic and energy efficiencies and increasing the operating voltage may also contribute to the improvement of the practical gravimetric energy density. Comparison of formic acid fuel cell and ammonium formate fuel cell is shown in Table S3. Therefore, despite the similar maximum power densities of the ammonium formate and DFFC, from the perspective of efficiency, the remarkably higher energy efficiency of the ammonium formate fuel cell verifies our hypothesis that the ammonium ion could contribute to the electricity generation. When a lower discharging current density of 50.0 mA cm^{-2} is employed, the ammonium formate fuel cell could maintain a longer operation exceeding 90 h (Figure S4). Under this situation, the Faradaic efficiency, energy efficiency, and gravimetric energy density are upgraded to 75.8%, 13.4%, and 1312 J g^{-1}, respectively. This phenomenon indicates that a lower current density prolongs the cell operation, such that it can make more use of the fuel. The discharging behavior shows that the voltage of ammonium formate fuel cell occasionally recovers, which is rare in similar tests. Hence, the operando potential is detected by including a reference electrode in this fuel cell system. As shown in Figure 3e, the cell voltage fluctuation is consistent with the anode potential, which means that the sole reason for the voltage recovery is that the anode potential becomes more negative. The reason for this phenomenon might be explained by the two-phase counter flow on the anode. Since the anode reaction involves gas

evolution, the generated gas bubbles may be attached on the catalyst surface to cover the active sites, and accumulated in the porous electrode to block the reactant supply. Once the gas bubbles are swept out from the cell, the active sites will be exposed and delivery channels will be unchoked again, both of which are beneficial for maintaining a lower anode potential. In addition, the anode potential ranges from -0.7 V to -0.3 V, confirming that the anode is at a low potential region during cell operation. As a consequence, the power density of ammonium formate fuel cell slightly falls behind the formate fuel cell, which is consistent with CV results. Obtaining the anode potential allows the voltage loss of the ammonium formate fuel cell to be analyzed, as shown in Figure 3f. The theoretical anode and cathode potentials are -0.91 V and 0.4 V, respectively, and they maintain constant at all current densities. The anode potential is determined by operando detection, while the anode polarization is calculated as the difference between the anode potential and theoretical potential. Similarly, the cathode potential is calculated, and the cathode polarization is the difference between the cathode potential and theoretical potential.[39] The results revealed that both anode and cathode polarizations are significant, with cathode polarization slightly higher than the anode polarization. Additionally, in the low current region, the ohmic loss is negligible whereas it becomes more pronounced in the high current region.

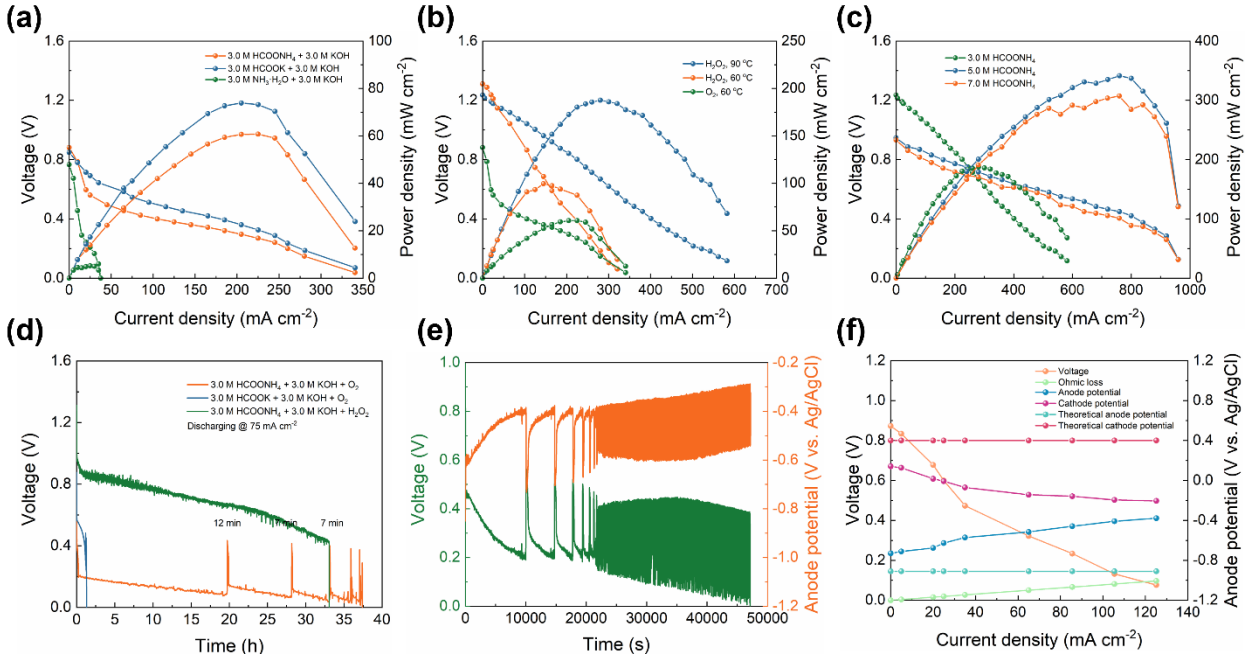

Figure 3. (a) Polarization and power density curves of the cell using different fuels. (b) Polarization and power density curves of different oxidants and temperatures. (c) Polarization and power density curves of different ammonium formate concentrations. (d) Constant-current discharging behavior of the fuel cell using different fuels. (e) Operando electrode potential detection. (f) Voltage losses of ammonium foramte fuel cell.

To track this process with complicated transportations and electrochemical reactions, a mathematical model is developed. The full set of parameters are listed in Tables S4-S7. Figures 4a and 4b depict the validation results of ammonium formate fuel cells using oxygen and hydrogen peroxide as oxidants, with individual voltage losses shaded. The simulation results exhibit excellent agreement with the experiment results, indicating that the developed model is a useful tool for studying voltage losses in ammonium formate fuel cells. For the cell with pure oxygen as

oxidant, the anode loss is the largest source of voltage loss (0.61 V at 3000 A m^{-2}), and the cathode loss is the second-largest source (0.47 V at 3000 A m^{-2}).[40] In contrast, for the cell with hydrogen peroxide as oxidant, the cathode loss is the largest source of voltage loss (as high as 1.08 V at 3000 A m^{-2}) and the anode loss is the second-largest source (0.61 V at 3000 A m^{-2}). The severe loss is caused by the spontaneous establishment of an internal hydrogen peroxide-based fuel cells due to hydrogen peroxide self-decomposition.[37] Ohmic loss is also present in both cases, while it is much smaller compared to electrode overpotentials.[41] Therefore, the synthesis of an appropriate and efficient electrocatalyst for both anode and cathode is crucial for future direction.[42]

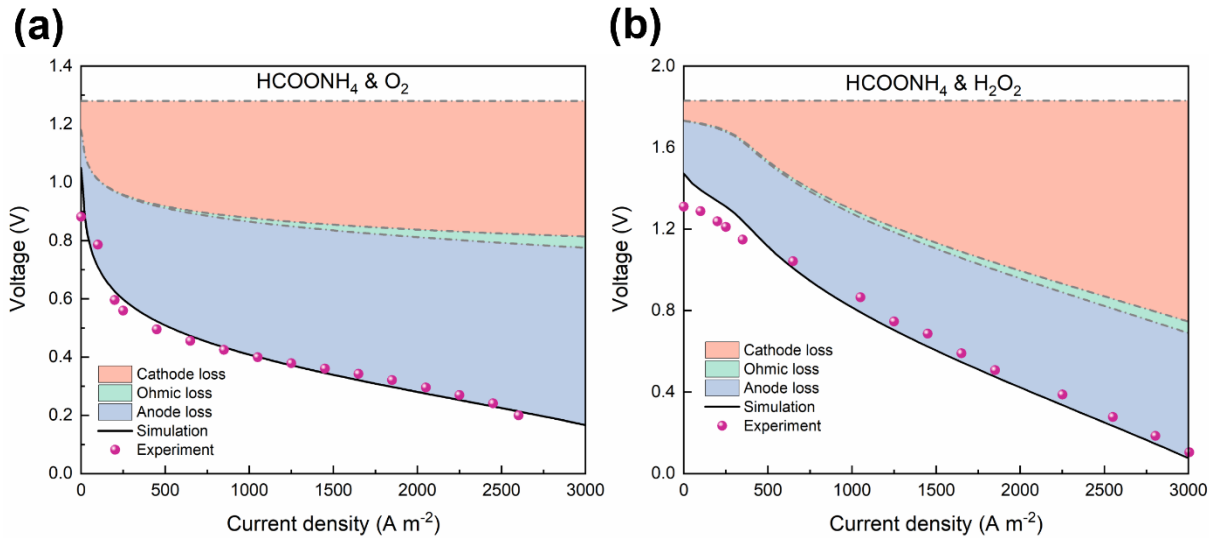

Figure 4. (a) Validation and simulation of ammonium formate fuel cell using pure oxygen. (b) Validation and simulation of ammonium formate fuel cell using hydrogen peroxide.

In this work, we develop an ammonium formate fuel cell which combines the advantages of formate with the ability of ammonium to release electrons for electricity generation. This ammonium formate fuel cell achieves impressive peak power density and OCV values of 61 mW

cm^{-2} and 0.88 V at 60 ºC, respectively. These values are further improved by substituting pure oxygen with hydrogen peroxide as an oxidant, resulting in power density and OCV values of 100 mW cm^{-2} and 1.31 V, respectively. A further increase of the operating temperature from to 90 ºC significantly enhances the power density to 188 mW cm^{-2}, and further to 337 mW cm^{-2} by increasing ammonium formate concentration. The efficiencies of this fuel cell, including Faradaic efficiency, energy efficiency, and gravimetric energy density are characterized to be 69.9%, 6.4%, and 6289 J g^{-1} (Figure S5), respectively, all of which outperform those of the formate fuel cell (6.2%, 2.6%, and 69 J g^{-1}). In addition, the operando potential detection reveal that the voltage recovery is due to the anode potential becoming more negative, indicating that the PtPd/C has a self-purge ability to remove the adsorbed intermediate of ammonium formate oxidation on the active sites, and thus exposing them again. Finally, our mathematical model show that using pure oxygen as oxidant, the anode loss was the largest source of voltage loss (0.61 V at 3000 A m^{-2}), followed by the cathode loss (0.47 V at 3000 A m^{-2}). When using hydrogen peroxide as oxidant, the cathode loss is the largest source of voltage loss (as high as 1.08 V at 3000 A m^{-2}), and the anode loss is the second-largest source (0.61 V at 3000 A m^{-2}). These findings highlight the need for an appropriate and efficient electrocatalyst for both the anode and cathode to further improve the performance of the ammonium formate fuel cell.

SUPPORTING INFORMATION

Experimental details of materials, preparation of PtPd/C, characterization of PtPd/C, preparation of membrane electrode assemblies, cyclic voltammetry and linear sweep voltammetry, fuel cell setup and instrumentation, energy efficiency and energy density of direct liquid fuel cells from open literature, theoretical voltage of ammonium formate/ hydrogen peroxide fuel cell, mathematical modeling, amount and selectivity of ammonium oxidation, PtPd/C stability, constant-current discharging behaviour, cell efficiency comparison, and tables for economic analysis, cell performance comparison and physiochemical parameters.

AUTHOR INFORMATION

Corresponding Authors

Qixing Wu - Shenzhen Key Laboratory of New Lithium-ion Batteries and Mesoporous Materials, College of Chemistry and Environmental Engineering, Shenzhen University, Shenzhen, 518060, China, Email: qxwu@szu.edu.cn

Liang An - Department of Mechanical Engineering, The Hong Kong Polytechnic University, Hung Hom, Kowloon, Hong Kong SAR, China, Email: liang.an@polyu.edu.hk

Authors

Zhefei Pan - Department of Mechanical Engineering, The Hong Kong Polytechnic University, Hung Hom, Kowloon, Hong Kong SAR, China

Zhewei Zhang - Department of Mechanical Engineering, The Hong Kong Polytechnic University, Hung Hom, Kowloon, Hong Kong SAR, China

Wenzhi Li - Department of Mechanical Engineering, The Hong Kong Polytechnic University, Hung Hom, Kowloon, Hong Kong SAR, China

Xiaoyu Huo - Department of Mechanical Engineering, The Hong Kong Polytechnic University, Hung Hom, Kowloon, Hong Kong SAR, China

Yun Liu - Department of Mechanical Engineering, The Hong Kong Polytechnic University, Hung Hom, Kowloon, Hong Kong SAR, China

Oladapo Christopher Esan - Department of Mechanical Engineering, The Hong Kong Polytechnic University, Hung Hom, Kowloon, Hong Kong SAR, China

Notes

The authors declare no competing financial interest.

ACKNOWLEDGMENT

The work described in this paper was supported by a grant from the Research Grants Council of the Hong Kong Special Administrative Region, China (No. N_PolyU559/21) and grants from the Shenzhen Science and Technology Program (No. SGDX20201103095204 04, No. JCYJ20190808123011253).

REFERENCES

(1) Zhao, T. S.; Xu, C.; Chen, R.; Yang, W. W. Mass transport phenomena in direct methanol fuel cells. *Prog. Energy Combust. Sci.* **2009**, *35* (3), 275-292.

(2) Pan, Z. F.; An, L.; Zhao, T. S.; Tang, Z. K. Advances and challenges in alkaline anion exchange membrane fuel cells. *Prog. Energy Combust. Sci.* **2018**, *66*, 141-175.

(3) An, L.; Zhao, T. S.; Li, Y. S. Carbon-neutral sustainable energy technology: Direct ethanol fuel cells. *Renewable Sustainable Energy Rev.* **2015**, *50*, 1462-1468.

(4) Su, X.; Pan, Z.; An, L. Three-dimensional porous electrodes for direct formate fuel cells. *Science China Technological Sciences* **2021**, *64* (4), 705-718.

(5) Su, X.; Pan, Z.; An, L.; Yu, Y. Mathematical modeling of direct formate fuel cells incorporating the effect of ion migration. *Int. J. Heat Mass Transfer* **2021**, *164*, 120629.

(6) Pan, Z. F.; An, L.; Wen, C. Y. Recent advances in fuel cells based propulsion systems for unmanned aerial vehicles. *Appl. Energy* **2019**, *240*, 473-485.

(7) Yazdani, A.; Botte, G. G. Perspectives of electrocatalysis in the chemical industry: a platform for energy storage. *Curr. Opin. Chem. Eng.* **2020**, *29*, 89-95.

(8) Busó-Rogero, C.; Ferre-Vilaplana, A.; Herrero, E.; Feliu, J. M. The role of formic acid/formate equilibria in the oxidation of formic acid on Pt (111). *Electrochem. Commun.* **2019**, *98*, 10-14.

(9) Ferre-Vilaplana, A.; Perales-Rondón, J. V.; Buso-Rogero, C.; Feliu, J. M.; Herrero, E. Formic acid oxidation on platinum electrodes: a detailed mechanism supported by experiments and calculations on well-defined surfaces. *J. Mater. Chem. A* **2017**, *5* (41), 21773-21784.

(10) Bienen, F.; Kopljar, D.; Löwe, A.; Aßmann, P.; Stoll, M.; Rößner, P.; Wagner, N.; Friedrich, A.; Klemm, E. Utilizing formate as an energy carrier by coupling CO_2 electrolysis with fuel cell devices. *Chem. Ing. Tech.* **2019**, *91* (6), 872-882.

(11) Pan, Z.; Liu, Y.; Tahir, A.; Christopher Esan, O.; Zhu, J.; Chen, R.; An, L. A discrete regenerative fuel cell mediated by ammonia for renewable energy conversion and storage. *Appl. Energy* **2022**, *322*, 119463.

(12) Pan, Z.; Khalid, F.; Tahir, A.; Esan, O. C.; Zhu, J.; Chen, R.; An, L. Water flooding behavior in flow cells for ammonia production via electrocatalytic nitrogen reduction. *Fundamental Research* **2022**, *2* (5), 757-763.

(13) Pan, Z.; Zhang, Z.; Tahir, A.; Esan, O. C.; Liu, X.; Wang, H.; An, L. Ultralow loading FeCoNi alloy nanoparticles decorated carbon mat for hydrogen peroxide reduction reaction and its application in direct ethylene glycol fuel cells. *Int. J. Energy Res.* **2022**, *46* (10), 13820-13831.

(14) Schiffer, Z. J.; Biswas, S.; Manthiram, K. Ammonium formate as a safe, energy-dense electrochemical fuel ionic liquid. *ACS Energy Lett.* **2022**, *7* (10), 3260-3267.

(15) Liu, H.; Chen, Y.; Lee, J.; Gu, S.; Li, W. Ammonia-mediated CO_2 capture and direct electroreduction to formate. *ACS Energy Lett.* **2022**, *7* (12), 4483-4489.

(16) Xu, T. Ion exchange membranes: State of their development and perspective. *J. Membr. Sci.* **2005**, *263* (1), 1-29.

(17) Dekel, D. R. Review of cell performance in anion exchange membrane fuel cells. *J. Power Sources* **2018**, *375*, 158-169.

(18) Pan, Z.; Bi, Y.; An, L. A cost-effective and chemically stable electrode binder for alkaline-acid direct ethylene glycol fuel cells. *Appl. Energy* **2020**, *258*, 114060.

(19) Pan, Z. F.; Chen, R.; An, L.; Li, Y. S. Alkaline anion exchange membrane fuel cells for cogeneration of electricity and valuable chemicals. *J. Power Sources* **2017**, *365*, 430-445.

(20) Ohyama, K.; Kimura, C.; Aoki, H.; Kuwabata, S.; Sugino, T. Evaluation of solid ammonium formate oxidation for PEM fuel cells. *ECS Trans.* **2007**, *11* (1), 1473-1477.

(21) Ohyama, K.; Sugino, T.; Nitta, T.; Kimura, C.; Aoki, H. Improvement of anode oxidation reaction of a fuel cell using ammonium formate with Pt-Ir catalysis. *Electr. Eng. Jpn.* **2011**, *174* (4), 45-50.

(22) Aoki, H.; Nitta, T.; Kuwabata, S.; Kimura, C.; Sugino, T. Improvement of anode oxidation reaction of a fuel cell using ammonium formate with Pt-Pd catalysts. *ECS Trans.* **2008**, *16* (2), 849-853.

(23) Takamura, T.; Mochimaru, F. Adsorption and oxidation of formate on palladium in alkaline solution. *Electrochim. Acta* **1969**, *14* (1), 111-119.

(24) John, J.; Wang, H.; Rus, E. D.; Abruña, H. D. Mechanistic studies of formate oxidation on platinum in alkaline medium. *J. Phys. Chem. C* **2012**, *116* (9), 5810-5820.

(25) Pan, Z.; Liu, Y.; Zhang, Z.; Zhao, Z.; Zhu, J.; Chen, R.; An, L. A bifunctional electrochemical flow cell integrating ammonia production and electricity generation for renewable energy conversion and storage. *Int. J. Hydrogen Energy* **2022**, *47* (90), 38361-38371.

(26) Guo, Y.; Pan, Z.; An, L. Carbon-free sustainable energy technology: Direct ammonia fuel cells. *J. Power Sources* **2020**, *476*, 228454.

(27) Liu, H.-Y.; Lant, H. M. C.; Troiano, J. L.; Hu, G.; Mercado, B. Q.; Crabtree, R. H.; Brudvig, G. W. Electrocatalytic, homogeneous ammonia oxidation in water to nitrate and nitrite with a copper complex. *J. Am. Chem. Soc.* **2022**, *144* (19), 8449-8453.

(28) Choueiri, R. M.; Tatarchuk, S. W.; Klinkova, A.; Chen, L. D. Mechanism of ammonia oxidation to dinitrogen, nitrite, and nitrate on β-$Ni(OH)_2$ from first-principles simulations. *Electrochemical Science Advances* **2022**, *2* (6), e2100142.

(29) Zhang, H.; Xu, L.; Tian, Y.; Jiao, A.; Li, S.; Liu, X.; Chen, M.; Chen, F. Convenient synthesis of 3D fluffy PtPd nanocorals loaded on 2D h-BN supports as highly efficient and stable electrocatalysts for alcohol oxidation reaction. *ACS Omega* **2019**, *4* (6), 11163-11172.

(30) Feng, L.; Si, F.; Yao, S.; Cai, W.; Xing, W.; Liu, C. Effect of deposition sequences on electrocatalytic properties of PtPd/C catalysts for formic acid electrooxidation. *Catal. Commun.* **2011**, *12* (8), 772-775.

(31) Chu, Y.-Y.; Wang, Z.-B.; Jiang, Z.-Z.; Gu, D.-M.; Yin, G.-P. Facile synthesis of hollow spherical sandwich PtPd/C catalyst by electrostatic self-assembly in polyol solution for methanol electrooxidation. *J. Power Sources* **2012**, *203*, 17-25.

(32) Pan, Z.; Zhuang, H.; Bi, Y.; An, L. A direct ethylene glycol fuel cell stack as air-independent power sources for underwater and outer space applications. *J. Power Sources* **2019**, *437*, 226944.

(33) Zhao, Y.; Setzler, B. P.; Wang, J.; Nash, J.; Wang, T.; Xu, B.; Yan, Y. An efficient direct ammonia fuel cell for affordable carbon-neutral transportation. *Joule* **2019**, *3* (10), 2472-2484.

(34) Zhao, Y.; Wang, T.; Setzler, B. P.; Abbasi, R.; Wang, J.; Yan, Y. A high-performance gas-fed direct ammonia hydroxide exchange membrane fuel cell. *ACS Energy Lett.* **2021**, *6* (5), 1996-2002.

(35) Pan, Z.; Bi, Y.; An, L. Performance characteristics of a passive direct ethylene glycol fuel cell with hydrogen peroxide as oxidant. *Appl. Energy* **2019**, *250*, 846-854.

(36) Wang, Z.; Mandal, M.; Sankarasubramanian, S.; Huang, G.; Kohl, P. A.; Ramani, V. K. Influence of water transport across microscale bipolar interfaces on the performance of direct borohydride fuel cells. *ACS Appl. Energy Mater.* **2020**, *3* (5), 4449-4456.

(37) Pan, Z.; Bi, Y.; An, L. Mathematical modeling of direct ethylene glycol fuel cells incorporating the effect of the competitive adsorption. *Appl. Therm. Eng.* **2019**, *147*, 1115-1124.

(38) Liu, J. G.; Zhao, T. S.; Chen, R.; Wong, C. W. The effect of methanol concentration on the performance of a passive DMFC. *Electrochem. Commun.* **2005**, *7* (3), 288-294.

(39) Ioroi, T.; Siroma, Z.; Yamazaki, S.-i.; Yasuda, K. Electrocatalysts for PEM fuel cells. *Adv. Energy Mater.* **2019**, *9* (23), 1801284.

(40) Dekel, D. R.; Yassin, K.; Rasin, I. G.; Brandon, S. Modeling direct ammonia anion-exchange membrane fuel cells. *J. Power Sources* **2023**, *558*, 232616.

(41) Varcoe, J. R.; Atanassov, P.; Dekel, D. R.; Herring, A. M.; Hickner, M. A.; Kohl, P. A.; Kucernak, A. R.; Mustain, W. E.; Nijmeijer, K.; Scott, K.; et al. Anion-exchange membranes in electrochemical energy systems. *Energy Environ. Sci.* **2014**, *7* (10), 3135-3191.

(42) Pan, Z.; Huang, B.; An, L. Performance of a hybrid direct ethylene glycol fuel cell. *Int. J. Energy Res.* **2019**, *43* (7), 2583-2591.